

Article

# Nonlinear Optimal Control Law of Autonomous Unmanned Surface Vessels

Yung-Yue Chen \*, Chun-Yen Lee, Shao-Han Tseng and Wei-Min Hu \*

Department of Systems and Naval Mechatronic Engineering, Tainan National Cheng Kung University, Tainan 70101, Taiwan; P18081013@mail.ncku.edu.tw (C.-Y.L.); kuchikiyorugin@gmail.com (S.-H.T.)

\* Correspondence: yungyuchen@mail.ncku.edu.tw (Y.-Y.C.); aaa09725@hotmail.com (W.-M.H.);  
Tel.: +886-912186952 and 886-972313955

Received: 19 January 2020; Accepted: 21 February 2020; Published: 2 March 2020

**Abstract:** For energy conservation, nonlinear-optimal-control-law design for marine surface vessels has become a crucial ocean technology for the current ship industry. A well-controlled marine surface vessel with optimal properties must possess accurate tracking capability for accomplishing sailing missions. To achieve this design target, a closed-form nonlinear optimal control law for the trajectory- and waypoint-tracking problem of autonomous marine surface vessels (AUSVs) is presented in this investigation. The proposed approach, based on the optimal control concept, can be effectively applied to generate control commands on marine surface vessels operating in sailing scenarios where ocean environmental disturbances are random and unpredictable. In general, it is difficult to directly obtain a closed-form solution from this optimal tracking problem. Fortunately, by having the adequate choice of state-variable transformation, the nonlinear optimal tracking problem of autonomous marine surface vessels can be converted into a solvable nonlinear time-varying differential equation. The solved closed-form solution can also be acquired with an easy-to-implement control structure for energy-saving purposes.

**Keywords:** nonlinear control law; tracking design; closed-form solution; optimal performance index

---

## 1. Introduction

The ocean is an unknown, challenging, and mysterious territory. In order to complete given missions, researchers explore the ocean using multiple methods and equipment, such as using unmanned aerial vehicles and research ships. However, these methods may have several drawbacks, such as huge financial pressure and time-consuming operation processes for ocean message searching. To resolve these mentioned difficulties, throughout the past few decades, researchers have developed new exploration vehicles, autonomous unmanned surface vessels (AUSVs), to navigate the ocean. Control-system design is a key function of AUSVs that allows them to successfully achieve tracking missions. The main design challenge for the tracking problem of AUSVs during the execution of sailing missions or the acquisition of sea resources is how to precisely guide AUSVs to designated locations while consuming low power. For collecting long-term data while consuming low power in an unpredictable ocean environment, designing an effective nonlinear optimal control law is essential for AUSVs. Until now, numerous researchers tried to overcome this challenge by developing proper and effective control methods. Many existing studies for the trajectory-tracking problem of AUSVs were proposed, such as [1,2], which proposed linear control methods that are only capable of treating scenarios with certain operation points. These kinds of linear control designs usually work weakly in global ocean environments. Several studies for trajectory-tracking design have been proposed. Some of them are nonlinear control investigations based on sliding-control perspectives, which may possess global characteristics for the autonomous design of AUSVs [3,4].

However, the conservation features (high control gain) of control forces and the applied torque, as well as an inevitable system-chattering character, always appear in AUSVs. In [5,6], two adaptive-based control approaches with adjustable weights that should be optimized were investigated for AUSVs. In [7], a backstepping control method for treating the stabilization and tracking problem of AUSVs under the effect of constant-bias ocean-environment disturbances was studied. A backstepping Type 2 fuzzy control design with a series of decision-making procedures was proposed in [8]. The authors proposed nonlinear control designs for the trajectory-tracking problem of AUSVs [9,10]. These control designs are usually too complicated in control structure, resulting in relatively huge power consumption for calculations in each mission. To reduce calculation-power consumption and develop an easy-to-implement control structure, two concise control laws were proposed based on the linear-algebra approach and experiment tests for AUSVs in [11,12]. In these two control achievements, trajectory-tracking performance was well-considered, but the energy-saving problem of AUSVs was not considered in the control-design process. Closed-form nonlinear optimal control design of AUSVs remedies the aforementioned problems. However, an optimal closed-form solution of trajectory- and waypoint-tracking problems of AUSVs have not yet been solved because of the extremely complex dynamics between controlled AUSVs and random ocean environments. To simplify the control structure and precisely guide AUSVs to the desired destinations, an important contribution of this research is finding an optimal closed-form solution that has the simplest control structure for the trajectory- and waypoint-tracking problems of AUSVs. This paper is organized as follows: in Section 2, the mathematical expression of the marine-surface-vessel model and the design objective are given; in Section 3, the proposed optimal control law design is derived; in Section 4, the simulation results of the trajectory- and waypoint-tracking scenarios with modelling uncertainties and ocean-environment disturbances are shown and discussed; in the last section of the paper, the major conclusion of this investigation is stated.

## 2. Mathematical Model and Design Objective

### 2.1. Rigid-Body AUSV Dynamics

For the global tracking design purpose, nonlinear AUSV dynamics is formulated as the Earthfixed vector representation [13]:

$$M_{\eta}(\boldsymbol{\eta})\ddot{\boldsymbol{\eta}} + C_{\eta}(\boldsymbol{\beta}, \boldsymbol{\eta})\dot{\boldsymbol{\eta}} + D_{\eta}(\boldsymbol{\eta})\dot{\boldsymbol{\eta}} = \boldsymbol{\tau}_{\eta} + \boldsymbol{\tau}_{d\eta}(\boldsymbol{\eta}), \tag{1}$$

where  $\boldsymbol{\eta}=[x \ y \ \psi]$  contains positions ( $x$  and  $y$ ) in the  $x$ - $y$  axis and the yaw angle ( $\psi$ ) of the controlled AUSV in the global co-ordinate, and  $\boldsymbol{\beta}=[u \ v \ r]$  contains linear velocities  $u$  and  $v$ , and angular velocity  $r$  of the controlled AUSV in the body co-ordinate, respectively, as shown in Figure 1.

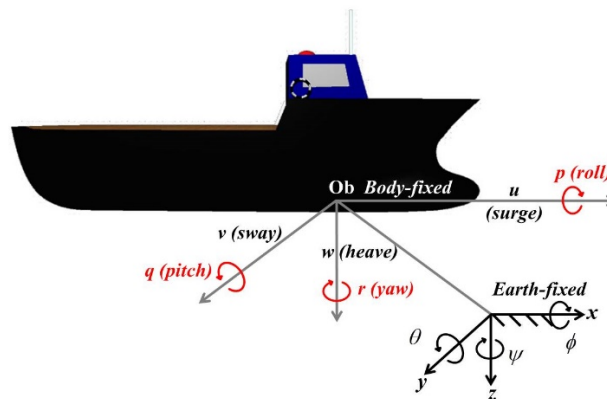


**Figure 1.** Body-frame and Earth frame definitions of controlled autonomous unmanned surface vessels (AUSV).

where  $\mathbf{M}_\eta(\boldsymbol{\eta}) = \mathbf{J}^{-T}(\boldsymbol{\eta})\mathbf{M}\mathbf{J}^{-1}(\boldsymbol{\eta})$  is the inertia mass,  $\mathbf{C}_\eta(\boldsymbol{\beta}, \boldsymbol{\eta}) = \mathbf{J}^{-T}(\boldsymbol{\eta})[\mathbf{C}(\boldsymbol{\beta}) - \mathbf{M}\mathbf{J}^{-1}(\boldsymbol{\eta})\dot{\mathbf{J}}(\boldsymbol{\eta})]\mathbf{J}^{-1}(\boldsymbol{\eta})$  is the Coriolis and centripetal matrix,  $\mathbf{D}_\eta(\boldsymbol{\eta}) = \mathbf{J}^{-T}(\boldsymbol{\eta})\mathbf{D}(\boldsymbol{\beta})\mathbf{J}^{-1}(\boldsymbol{\eta})$  is the damping matrix,  $\boldsymbol{\tau}_\eta(\boldsymbol{\eta}) = \mathbf{J}^{-T}(\boldsymbol{\eta})\boldsymbol{\tau}_{input}$  is the control input, and  $\boldsymbol{\tau}_{d\eta}(\boldsymbol{\eta}) = \mathbf{J}^{-T}(\boldsymbol{\eta})\boldsymbol{\tau}_{disturbances}$  is the ocean-environment disturbances in the global co-ordinate, respectively. System parameter matrices  $\mathbf{M}$ ,  $\mathbf{C}(\boldsymbol{\beta})$ ,  $\mathbf{D}(\boldsymbol{\beta})$ , and transformation matrix  $\mathbf{J}(\boldsymbol{\eta})$  are denoted as the following:

$$\mathbf{M} = \begin{bmatrix} m - X_u & 0 & 0 \\ 0 & m - Y_v & mx_g - Y_r \\ 0 & mx_g - N_v & I_z - N_r \end{bmatrix}$$

$$\mathbf{C}(\boldsymbol{\beta}) = \begin{bmatrix} 0 & 0 & -(m - Y_v)v - (mx_g - Y_r)r \\ 0 & 0 & (m - X_u)u \\ (m - Y_v)v + (mx_g - Y_r)r & -(m - X_u)u & 0 \end{bmatrix}$$

$$\mathbf{D}(\boldsymbol{\beta}) = \begin{bmatrix} -X_u & 0 & 0 \\ 0 & -Y_v & -Y_r \\ 0 & -N_v & -N_r \end{bmatrix}, \quad \mathbf{J}(\boldsymbol{\eta}) = \begin{bmatrix} \cos\psi & -\sin\psi & 0 \\ \sin\psi & \cos\psi & 0 \\ 0 & 0 & 1 \end{bmatrix},$$

where  $\mathbf{M} = \mathbf{M}^T > 0$  is the rigid-body inertia matrix that includes added mass.  $\mathbf{C}(\boldsymbol{\beta}) = -\mathbf{C}^T(\boldsymbol{\beta})$ ,  $\forall \boldsymbol{\beta} \in \mathfrak{R}^6$  is the matrix of Coriolis and centripetal terms that includes added mass.  $\mathbf{D}(\boldsymbol{\beta}) > 0$ ,  $\forall \boldsymbol{\beta} \in \mathfrak{R}^6$  is the hydrodynamic damping matrix.  $\boldsymbol{\tau}_{input}$  is the control vector with forces and torque.  $\boldsymbol{\tau}_{disturbances}$  is the vector of forces and torques induced by wave, wind, and ocean currents.

The controlled dynamics of the AUSV in Equation (1) were obtained under the following assumptions.

When applying nonlinear optimal control to this tracking problem of controlled AUSVs, ocean-environment disturbances  $\boldsymbol{\tau}_{d\eta}(\boldsymbol{\eta})$  of the dynamic equation in Equation (1) were omitted. This is because the optimal control performance (optimal performance) of controlled AUSVs theoretically does not take this term into account. Consequentially, the dynamic equation of a controlled AUSV can be rewritten as below:

$$\mathbf{M}_\eta(\boldsymbol{\eta})\ddot{\boldsymbol{\eta}} + \mathbf{C}_\eta(\boldsymbol{\beta}, \boldsymbol{\eta})\dot{\boldsymbol{\eta}} + \mathbf{D}_\eta(\boldsymbol{\eta})\dot{\boldsymbol{\eta}} = \boldsymbol{\tau}_{\eta 2}, \tag{2}$$

where  $\boldsymbol{\tau}_{\eta 2}$  is the proposed nonlinear optimal control law, which is derived below.

To simplify the representation of the dynamic equation of a controlled AUSV, the second and third terms in the left-hand side of Equation (1) were merged. This results in Equation (2), which was rewritten as the following:

$$\mathbf{M}_\eta(\boldsymbol{\eta})\ddot{\boldsymbol{\eta}} + \mathbf{N}_\eta(\boldsymbol{\beta}, \boldsymbol{\eta})\dot{\boldsymbol{\eta}} = \boldsymbol{\tau}_{\eta 2}, \tag{3}$$

where  $\mathbf{N}_\eta(\boldsymbol{\beta}, \boldsymbol{\eta}) = \mathbf{C}_\eta(\boldsymbol{\beta}, \boldsymbol{\eta}) + \mathbf{D}_\eta(\boldsymbol{\eta})$ .

### 2.2. Problem Formulation

In this investigation, the convergence property of tracking errors between the controlled AUSVs and continuous trajectories or waypoints was proven.  $\boldsymbol{\eta}_d$  are the desired trajectories or waypoints that were assumed to be twice continuously differentiable functions  $\boldsymbol{\eta}_d \in C^2$ . On the basis of this definition, the desired velocity and acceleration vectors with respect to  $\boldsymbol{\eta}_d$  are expressed as  $\dot{\boldsymbol{\eta}}_d$  and  $\ddot{\boldsymbol{\eta}}_d$ , respectively.

Define the tracking-error vector between the controlled AUSVs and continuous trajectories or waypoints as follows:

$$\mathbf{e} = \begin{bmatrix} \dot{\tilde{\boldsymbol{\eta}}} \\ \tilde{\boldsymbol{\eta}} \end{bmatrix} = \begin{bmatrix} \dot{\boldsymbol{\eta}} - \dot{\boldsymbol{\eta}}_d \\ \boldsymbol{\eta} - \boldsymbol{\eta}_d \end{bmatrix}. \tag{4}$$

From Equation (3) and the tracking error described in Equation (4), tracking-error dynamics can be expressed systematically as:

$$\dot{\mathbf{e}} = \begin{bmatrix} -\mathbf{M}_\eta^{-1}(\boldsymbol{\eta})\mathbf{N}_\eta(\boldsymbol{\beta}, \boldsymbol{\eta}) & \mathbf{0}_{3 \times 3} \\ \mathbf{I}_{3 \times 3} & \mathbf{0}_{3 \times 3} \end{bmatrix} \mathbf{e} + \begin{bmatrix} -\ddot{\boldsymbol{\eta}}_d - \mathbf{M}_\eta^{-1}(\boldsymbol{\eta})\mathbf{N}_\eta(\boldsymbol{\beta}, \boldsymbol{\eta})\dot{\boldsymbol{\eta}}_d \\ \mathbf{0}_{3 \times 1} \end{bmatrix} + \begin{bmatrix} \mathbf{M}_\eta^{-1}(\boldsymbol{\eta})\boldsymbol{\tau}_{\eta_2} \\ \mathbf{0}_{3 \times 1} \end{bmatrix}. \tag{5}$$

The tracking-error dynamics in Equation (5) is generally difficult to analyze because of their complex structure. Therefore, proportional derivative filtered link  $\boldsymbol{\delta}_2(t)$  and state-space transformation matrix  $\mathbf{V}_2$ , featured below, were adopted to transform the tracking-error dynamics in Equation (5) into a more analyzable form.

$$\boldsymbol{\delta}_2(t) = \boldsymbol{\rho}_2 \dot{\tilde{\boldsymbol{\eta}}} + \boldsymbol{\Gamma}_2 \tilde{\boldsymbol{\eta}} \tag{6}$$

$$\mathbf{V}_2 = \begin{bmatrix} \mathbf{V}_{21} \\ \mathbf{V}_{22} \end{bmatrix} = \begin{bmatrix} \mathbf{V}_{211} & \mathbf{V}_{212} \\ \mathbf{0}_{3 \times 3} & \mathbf{I}_{3 \times 3} \end{bmatrix} = \begin{bmatrix} \boldsymbol{\rho}_2 \mathbf{I}_{3 \times 3} & \boldsymbol{\Gamma}_2 \\ \mathbf{0}_{3 \times 3} & \mathbf{I}_{3 \times 3} \end{bmatrix}, \tag{7}$$

where  $\boldsymbol{\rho}_2$  and  $\boldsymbol{\Gamma}_2 \in \mathbb{R}^{3 \times 3}$  are a designable positive scale and a positive definite matrix that can be chosen mathematically. By this arrangement, Equation (5) can be formulated as:

$$\dot{\mathbf{e}} = \mathbf{V}_2^{-1} \begin{bmatrix} \dot{\boldsymbol{\delta}}_2(t) \\ \dot{\tilde{\boldsymbol{\eta}}}(t) \end{bmatrix} = \mathbf{R}_{2V}(\mathbf{e}, t) \mathbf{e} + \mathbf{S}_{2V}(\mathbf{e}, t) [\boldsymbol{\rho}_2 (-\mathbf{T}_2(\mathbf{e}, t) + \boldsymbol{\tau}_{\eta_2})], \tag{8}$$

where  $\mathbf{R}_{2V}(\mathbf{e}, t) = \mathbf{V}_2^{-1} \begin{bmatrix} -\mathbf{M}_\eta^{-1}(\boldsymbol{\eta})\mathbf{N}_\eta(\boldsymbol{\beta}, \boldsymbol{\eta}) & \mathbf{0}_{3 \times 3} \\ \boldsymbol{\rho}_2^{-1} \mathbf{I}_{3 \times 3} & -\boldsymbol{\rho}_2^{-1} \boldsymbol{\Gamma}_2 \end{bmatrix} \mathbf{V}_2$ ,  $\mathbf{S}_{2V}(\mathbf{e}, t) = \mathbf{V}_2^{-1} \mathbf{S} \mathbf{M}_\eta^{-1}(\boldsymbol{\eta})$ ,

$$\mathbf{T}_2(\mathbf{e}, t) = \mathbf{M}_\eta(\boldsymbol{\eta})(\ddot{\boldsymbol{\eta}}_d - \boldsymbol{\rho}_2^{-1} \boldsymbol{\Gamma}_2 \dot{\tilde{\boldsymbol{\eta}}}) + \mathbf{N}_\eta(\boldsymbol{\beta}, \boldsymbol{\eta})(\dot{\boldsymbol{\eta}}_d - \boldsymbol{\rho}_2^{-1} \boldsymbol{\Gamma}_2 \tilde{\boldsymbol{\eta}}) \text{ with } \mathbf{S} = \begin{bmatrix} \mathbf{I}_{3 \times 3} \\ \mathbf{0}_{3 \times 3} \end{bmatrix}.$$

Choosing closed-form nonlinear optimal control law for the tracking problem of AUSVs was as follows:

$$\boldsymbol{\tau}_{\eta_2} = \mathbf{T}_2(\mathbf{e}, t) + \boldsymbol{\rho}_2^{-1} \mathbf{u}_2. \tag{9}$$

Substituting the nonlinear optimal control law in Equation (9) into Equation (8), modified nonlinear tracking-error dynamics is presented as:

$$\dot{\mathbf{e}} = \mathbf{R}_{2V}(\mathbf{e}, t) \mathbf{e} + \mathbf{S}_{2V}(\mathbf{e}, t) \mathbf{u}_2. \tag{10}$$

### 2.3. Nonlinear Optimal Trajectory- and Waypoint-Tracking Problem of AUSVs

Considering the nonlinear tracking-error dynamics in Equation (8), and given weighting matrices  $\mathbf{Q}_2$  and  $\mathbf{W}_2$ , the design objective of this investigation was to find closed-form nonlinear optimal control law  $\boldsymbol{\tau}_{\eta_2}$  such that the following optimal performance (optimal performance) could be analytically achieved.

$$J(\mathbf{u}_2^*) = \min_{\mathbf{u}_2} J(\mathbf{u}_2) = \min_{\mathbf{u}_2} \left[ \mathbf{e}^T(t_f) \mathbf{Q}_{2f} \mathbf{e}(t_f) + \int_0^{t_f} \left[ \mathbf{e}^T(t) \mathbf{Q}_2 \mathbf{e}(t) + \mathbf{u}_2^T(t) \mathbf{W}_2 \mathbf{u}_2(t) \right] dt \right] = \mathbf{e}^T(0) \mathbf{P}_2(\mathbf{e}(0), 0) \mathbf{e}(0) \tag{11}$$

for all  $t_f \in [0, \infty]$  and  $\mathbf{Q}_{2f} = \mathbf{Q}_{2f}^T > 0$ .

## 3. Results

In this section, nonlinear closed-form optimal control law is delivered theoretically. The control objective was to find a nonlinear optimal control law to guide a controlled AUSV that could precisely track a designed trajectory or a set of waypoints with minimal power consumption. After

mathematical derivations, one main result based on the nonlinear optimal control concept could be derived as the following.

Closed-form nonlinear optimal control law that could optimally and precisely guide a controlled AUSV to track desired trajectories and waypoints was obtained as

$$\boldsymbol{\tau}_{\eta 2} = \mathbf{T}_2(\mathbf{e}, t) + \boldsymbol{\rho}_2^{-1} \mathbf{u}_2^*, \tag{12}$$

where  $\mathbf{u}_2^*(\mathbf{e}, t) = -\mathbf{W}_2^{-1} \mathbf{S}_{2V}^T(\mathbf{e}, t) \mathbf{P}_2(\mathbf{e}, t) \mathbf{e}(t)$  can analytically solve the nonlinear optimal tracking problem in Equation (11) if  $\mathbf{P}_2(\mathbf{e}, t)$  of  $\mathbf{u}_2^*(\mathbf{e}, t)$  satisfies the following nonlinear time-varying differential equation.

$$\dot{\mathbf{P}}_2(\mathbf{e}, t) + \mathbf{P}_2(\mathbf{e}, t) \mathbf{R}_{2V}(\mathbf{e}, t) + \mathbf{R}_{2V}^T(\mathbf{e}, t) \mathbf{P}_2(\mathbf{e}, t) + \mathbf{Q}_2 - \mathbf{P}_2(\mathbf{e}, t) \mathbf{S}_{2V}(\mathbf{e}, t) \mathbf{W}_2^{-1} \mathbf{S}_{2V}^T(\mathbf{e}, t) \mathbf{P}_2(\mathbf{e}, t) = 0 \tag{13}$$

with  $\mathbf{P}_2(\mathbf{e}, t) = \mathbf{P}_2^T(\mathbf{e}, t) \geq 0$  and  $\mathbf{Q}_{2f} = \mathbf{P}_2(\mathbf{e}(t_f), t_f)$ .

**Proof.** See Appendix A. □

**Remark 1.** Suppose closed-form solution  $\mathbf{P}_2(\mathbf{e}, t)$  can be found from the above nonlinear time-varying differential Equation (13). Then, nonlinear optimal control law  $\boldsymbol{\tau}_{\eta 2}$  can be easily built up with a simple form. In general, the highly complex nonlinear time-varying differential equation, as shown in Equation (13), is difficult to use to mathematically find a closed-form solution. Hence, it would be an important contribution if a closed-form  $\mathbf{P}_2(\mathbf{e}, t)$  was analytically derived.

### 3.1. Closed-form Solution $\mathbf{P}_2(\mathbf{e}, t)$ of Nonlinear Time-Varying Differential Equation (13)

Without loss of generality, solution  $\mathbf{P}_2(\mathbf{e}, t)$  is represented as the following structure:

$$\mathbf{P}_2(\mathbf{e}, t) = \mathbf{V}_2^T \begin{bmatrix} \mathbf{M}_\eta(\mathbf{e}, t) & \mathbf{0}_{3 \times 3} \\ \mathbf{0}_{3 \times 3} & \mathbf{K}_2 \end{bmatrix} \mathbf{V}_2, \tag{14}$$

where  $\mathbf{K}_2$  is some positive definite symmetric constant matrix. In the following section, conditions for the existences of matrices  $\mathbf{V}_2$  and  $\mathbf{K}_2$  for the closed-form solution are detailed.

#### Closed-Form Solution $\mathbf{P}_2(\mathbf{e}, t)$ of the Optimal Tracking Problem of AUSVs

Consider the second and third terms on the left-hand side of nonlinear differential Equation (13). Using the system property in Equations (8) and (14), the following result can be derived:

$$\mathbf{P}_2(\mathbf{e}, t) \mathbf{R}_{2V}(\mathbf{e}, t) + \mathbf{R}_{2V}^T(\mathbf{e}, t) \mathbf{P}_2(\mathbf{e}, t) = \begin{bmatrix} \mathbf{0}_{3 \times 3} & \mathbf{K}_2 \\ \mathbf{K}_2 & \mathbf{0}_{3 \times 3} \end{bmatrix} + \mathbf{V}_2^T \begin{bmatrix} -\dot{\mathbf{M}}_\eta(\mathbf{e}, t) & \mathbf{0}_{3 \times 3} \\ \mathbf{0}_{3 \times 3} & \mathbf{0}_{3 \times 3} \end{bmatrix} \mathbf{V}_2. \tag{15}$$

The following result can be derived:

$$\mathbf{S}_{2V}^T(\mathbf{e}, t) \mathbf{P}_2(\mathbf{e}, t) = \mathbf{S}^T \mathbf{V}_2. \tag{16}$$

Equation (13) can be simplified by using the results of Equations (15) and (16) in the following equation:

$$\begin{bmatrix} \mathbf{0}_{3 \times 3} & \mathbf{K}_2 \\ \mathbf{K}_2 & \mathbf{0}_{3 \times 3} \end{bmatrix} + \mathbf{Q}_2 - \mathbf{V}_2^T \mathbf{S} \mathbf{W}_2^{-1} \mathbf{S}^T \mathbf{V}_2 = \mathbf{0}_{6 \times 6}. \tag{17}$$

From Equation (16), optimal value  $\mathbf{u}_2^*(\mathbf{e}, t)$  of the second term of the nonlinear optimal control law  $\boldsymbol{\tau}_{\eta 2}$  in Equation (9) can be further formulated as:

$$\mathbf{u}_2^*(\mathbf{e}, t) = -\mathbf{W}_2^{-1} \mathbf{S}^T \mathbf{V}_2 \mathbf{e}. \tag{18}$$

### 3.2. Derivations of Optimal Parameters $\mathbf{W}_2$ and $\mathbf{V}_2$ for $\mathbf{u}_2^*(\mathbf{e}, t)$

By choosing

$$\mathbf{W}_2 = a_2^2 \mathbf{I}_{3 \times 3}, \tag{19}$$

$a_2 > 0$ .

Positive definite symmetric matrix  $\mathbf{Q}_2$  can also be factorized by Cholesky factorization as

$$\mathbf{Q}_2 = \begin{bmatrix} \mathbf{Q}_{211}^T \mathbf{Q}_{211} & \mathbf{Q}_{212} \\ \mathbf{Q}_{212}^T & \mathbf{Q}_{222}^T \mathbf{Q}_{222} \end{bmatrix} \tag{20}$$

By substituting matrices  $\mathbf{W}_2$ ,  $\mathbf{S}$  and  $\mathbf{Q}_2$  to Equation (17), the following equalities can be obtained:

$$\mathbf{Q}_{211}^T \mathbf{Q}_{211} - \frac{1}{a_2^2} \mathbf{V}_{211}^T \mathbf{V}_{211} = \mathbf{0}_{3 \times 3} \tag{21}$$

$$\mathbf{K}_2 + \mathbf{Q}_{212} - \frac{1}{a_2^2} \mathbf{V}_{211}^T \mathbf{V}_{212} = \mathbf{0}_{3 \times 3} \tag{22}$$

$$\mathbf{K}_2 + \mathbf{Q}_{212} - \frac{1}{a_2^2} \mathbf{V}_{212}^T \mathbf{V}_{211} = \mathbf{0}_{3 \times 3} \tag{23}$$

$$\mathbf{Q}_{222}^T \mathbf{Q}_{222} - \frac{1}{a_2^2} \mathbf{V}_{212}^T \mathbf{V}_{212} = \mathbf{0}_{3 \times 3} \tag{24}$$

By solving Equations (21) and (24), we get submatrices  $\mathbf{V}_{211} = a_2 \mathbf{Q}_{211}$  and  $\mathbf{V}_{212} = a_2 \mathbf{Q}_{222}$ . The matrix  $\mathbf{V}_2$  can then be expressed as:

$$\mathbf{V}_2 = \begin{bmatrix} a_2 \mathbf{Q}_{211} & a_2 \mathbf{Q}_{222} \\ \mathbf{0}_{3 \times 3} & \mathbf{I}_{3 \times 3} \end{bmatrix}. \tag{25}$$

For satisfying the condition of Equation (7), matrix  $\mathbf{Q}_{211}$  is expressed as a diagonal form as:

$$\mathbf{Q}_{211} = q_{211} \mathbf{I}_{3 \times 3}. \tag{26}$$

For some positive scale  $q_{211}$ , scale  $\rho_2$  for the optimal tracking problem of AUSVs can then be represented as

$$\rho_2 = a_2 q_{211}. \tag{27}$$

On the basis of the above derivations, weighting matrix  $\mathbf{W}_2$  was chosen as Equation (19) for any finite  $a_2 > 0$ , allowing weighting matrix  $\mathbf{Q}_2 > 0$  to be analyzed with  $\mathbf{Q}_{211}$ ,  $\mathbf{Q}_{212}$ , and  $\mathbf{Q}_{222}$ , which satisfies the requirements in Equations (25) and (26). The nonlinear optimal tracking problem of AUSVs is then solved by the following nonlinear optimal control law:

$$\boldsymbol{\tau}_{\eta_2} = \mathbf{T}_2(\mathbf{e}, t) + \boldsymbol{\rho}_2^{-1} \mathbf{u}_2^*(\mathbf{e}, t), \tag{28}$$

where

$$\mathbf{u}_2^*(\mathbf{e}, t) = -\frac{1}{a_2} [\mathbf{Q}_{211} \quad \mathbf{Q}_{222}] \mathbf{e}. \tag{29}$$

#### 4. Discussion

As stated in the introduction, AUSV parameters, ocean-environment disturbances, and control parameters for installing simulation scenarios and for verifying the control performance of this proposed method are listed below.

#### 4.1. Parameterizations of Controlled AUSV and Ocean-Environment Disturbances

Parameters of the dynamics of the controlled AUSV were given by Fossen [13]. Parameters of AUSV in Figure 2 and hydrodynamic parameters are exhibited in Table 1 and Table 2.

**Table 1.** Dimensions of the autonomous unmanned surface vessels (AUSV) illustrated in Figure 2.

Parameter	Value	SI Unit
Length ( $L$ )	76.2	m
Breadth ( $B$ )	30	m
Height ( $T$ )	20	m
Mass ( $m$ )	$4 \times 10^6$	kg
$x_g$	0	m

**Table 2.** Hydrodynamic parameters.

Parameter	Value	SI Unit
$I_z$	$2.0903 \times 10^9$	kgm <sup>2</sup>
$X_{\dot{u}}$	$-0.5096 \times 10^6$	kg
$Y_v$	$-0.1698 \times 10^6$	kg/s
$Y_{\dot{v}}$	$-3.5608 \times 10^6$	kg
$Y_r$	$1.5081 \times 10^6$	kgm/s
$Y_{\dot{r}}$	$-0.02268 \times 10^9$	kgm
$N_v$	$1.5081 \times 10^6$	kgm/s
$N_{\dot{v}}$	$-0.02268 \times 10^9$	kgm
$N_r$	$-0.2530 \times 10^9$	kgm <sup>2</sup> /s
$N_{\dot{r}}$	$-0.8780 \times 10^9$	kgm <sup>2</sup>

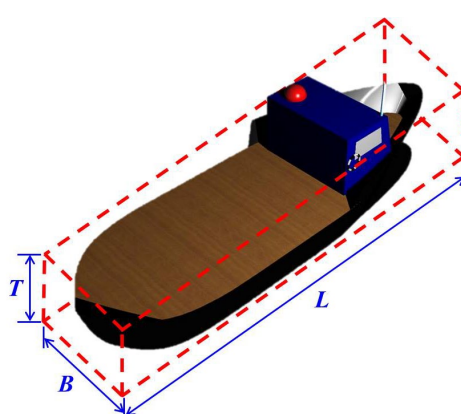


**Figure 2.** Principal dimensions of controlled AUSV.

By applying the values of Table 1 and Table 2, the dynamics-parameter matrices of the controlled AUSV are given below:

$$\mathbf{M} = \begin{bmatrix} 4.5096 & 0 & 0 \\ 0 & 7.5608 & -22.68 \\ 0 & -22.68 & 2968.3 \end{bmatrix} \times 10^6$$

$$\mathbf{D}(\boldsymbol{\beta}) = \begin{bmatrix} 0.05138 & 0 & 0 \\ 0 & 0.1698 & -1.5081 \\ 0 & -1.5081 & 253 \end{bmatrix} \times 10^6$$

$$\mathbf{C}(\boldsymbol{\beta}) = \begin{bmatrix} 0 & 0 & -7.5608v - 22.68r \\ 0 & 0 & 4.5096 \\ 7.5608v + 22.68r & -4.5096 & 0 \end{bmatrix} \times 10^6.$$

The perturbed uncertainties of the parameters of the AUSV were a random 5%–10% of inertial matrix  $\mathbf{M}_\eta$  and Coriolis matrix  $\mathbf{C}_\eta$ . The parameters of external disturbances—wind, wave and ocean current-induced forces and torques—are shown in Table 3, which are valid when the wind velocity is in the range of 2–3.96 m/s, and when encounter angles range from  $-180^\circ$  to  $180^\circ$ . Detailed values for simulating the environmental disturbances, including wind, wave and current, are listed as Table 3 [13].

**Table 3.** Modeling parameters of environmental disturbances (wind, wave, and current).

Parameter	Value	Parameter	Value
$V_w(m/s)$	3.96	$C_{Xw}(\gamma_R)$	$[-0.8 \ 1]$
$C_{Yw}(\gamma_R)$	$[-0.7 \ 1]$	$C_{Nw}(\gamma_R)$	$[-1.05 \ 1.05]$
$\rho_{air}(kg/m^3)$	1.1644	$\rho_w(kg/m^3)$	1025
$g(m/s^2)$	9.8	$N$	1000
$\beta$	$[-\pi \ \pi]$	$A_i$	3
$\phi_i$	$[0 \ 2\pi)$	$\lambda_i$	1

In Table 3,  $V_w(m/s)$  is the average wind speed above the ocean surface;  $C_{Xw}(\gamma_R)$ ,  $C_{Yw}(\gamma_R)$ , and  $C_{Nw}(\gamma_R)$  are nondimensional forces and moments induced by wind;  $\rho_{air}(kg/m^3)$  is air density;  $\rho_w(kg/m^3)$  is water density;  $g(m/s^2)$  is gravity acceleration;  $N$  is the order of the adopted wave form;  $\beta$  is the angle between the heading and the direction of the incoming wave;  $A_i$  is the wave amplitude of the  $i$ th wave component;  $\phi_i$  is the random phase of the  $i$ th wave component angle; and  $\lambda_i$  is the  $i$ th wave length.

#### 4.2. Control-Parameter Setup

Control parameters that satisfied the existence conditions in Equation (7) for the proposed nonlinear optimal control design are indicated in Table 4.

**Table 4.** Control parameters for optimal control design.

Parameter	Value
	0.002
$a_2$	0.005
	0.008
$\Gamma_2$	$\begin{bmatrix} 1 & 0 & 0 \\ 0 & 1 & 0 \\ 0 & 0 & 1 \end{bmatrix}$
$q_{211}$	50000

$$\begin{matrix} \mathbf{Q}_{211} & q_{211} \mathbf{I}_{3 \times 3} \\ \mathbf{Q}_{222} & \mathbf{I}_{3 \times 3} \end{matrix}$$

### 4.3. Simulation Results of Tracking Continuous Trajectory and Waypoints

To verify the control performance of the proposed optimal method to the AUSV, a scenario with a continuous circular trajectory and a scenario with eight waypoints were arranged.

**Scenario 1:** The predefined circular reference trajectory was generated by Equation (30) as below:

$$\begin{cases} x_d = x_0 + R \cos(\psi_d) \\ y_d = y_0 + R \sin(\psi_d) \end{cases} \quad (30)$$

where  $R$  is the radius of the desired circular trajectory, and  $\psi_d$  is a rotation angle that was integrated with constant angle velocity  $w_d$  as the following:

$$\psi_d = \int_0^t w_d dt . \quad (31)$$

On the basis of Equations (30) and (31), the desired trajectory can be expressed as  $\boldsymbol{\eta}_d = [x_d \ y_d \ \psi_d]$ .

The parameters for building up a circular trajectory are listed as Table 5, and the initial conditions of the controlled AUSV are given in Table 6.

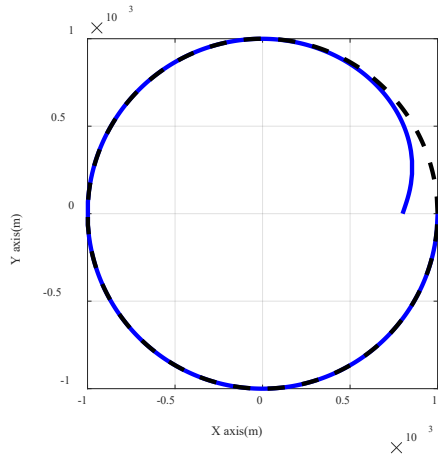
**Table 5.** Circular-trajectory parameters.

$x_o$ (m)	$y_o$ (m)	$w_d$ (rad/s)	$r$ (m)
0	0	$\pi / 900$	1000

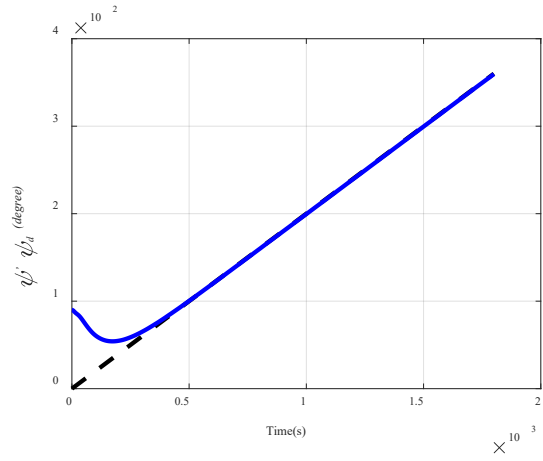
**Table 6.** Initial AUSV conditions (continuous trajectory).

$x$ (m)	$y$ (m)	$\psi$ (degree)
800	0	90°

Simulation results for tracking the desired circular trajectory are shown in Figures 3–6, based on parameters listed in Table 5 and Table 6. Figure 3a shows that the controlled AUSV tracked the desired circular trajectory from initial point  $\boldsymbol{\eta} = [800, 0, 90]$  using the proposed nonlinear optimal control law. Figure 4 shows that tracking errors  $e_x$ ,  $e_y$ , and  $e_\psi$  of the controlled AUSV in the X and Y axes, and yaw direction exponentially converged to zero, respectively, and these results indicated the promising tracking abilities of this proposed control law. The moving velocities and angle velocity of the controlled AUSV in the global co-ordinate are plotted in Figure 5.

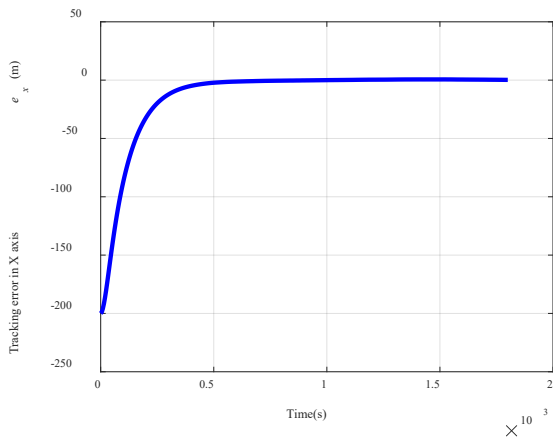


(a) Trajectory-tracking result of this proposed method with respect to desired trajectory.

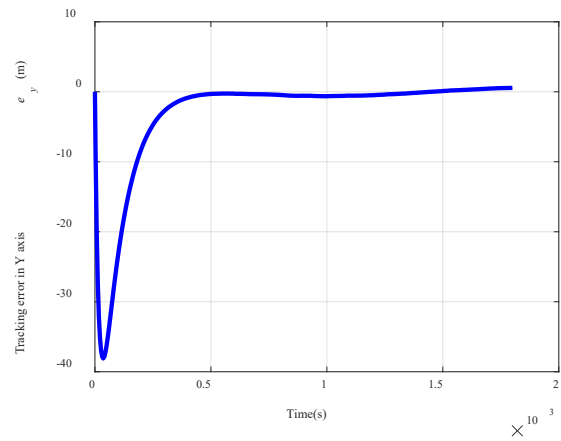


(b) Tracking histories of  $\psi$  with respect to  $\psi_d$ .

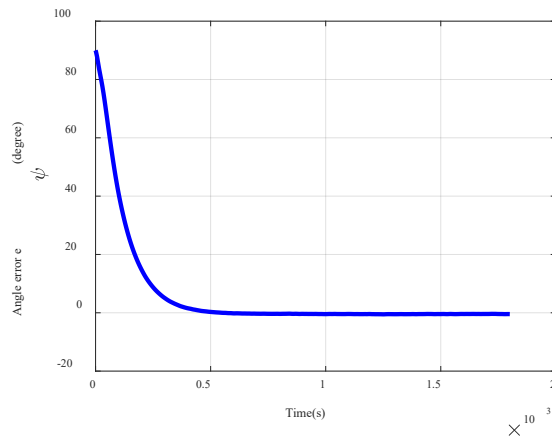
**Figure 3.** Tracking histories of controlled AUSV: proposed method (blue solid line) and desired trajectory (black dashed line).



(a) Tracking error in x axis.

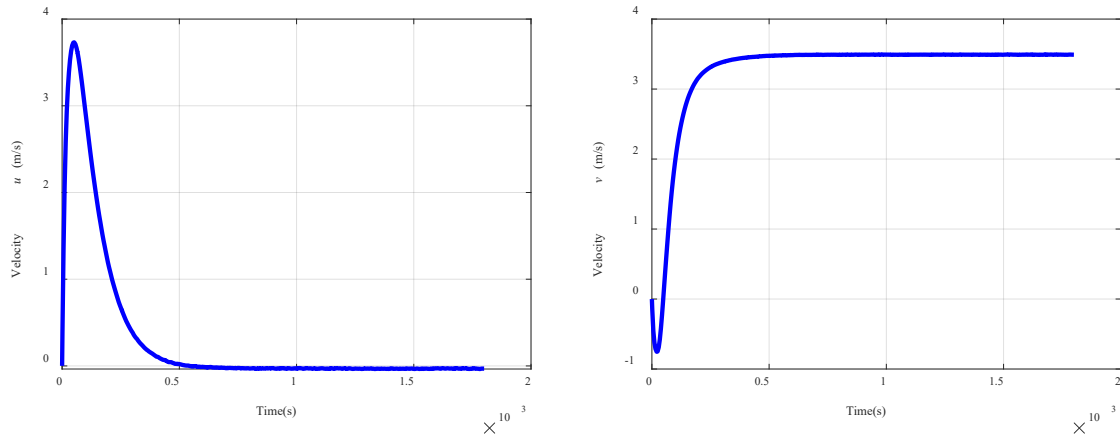


(b) Tracking error in y axis.



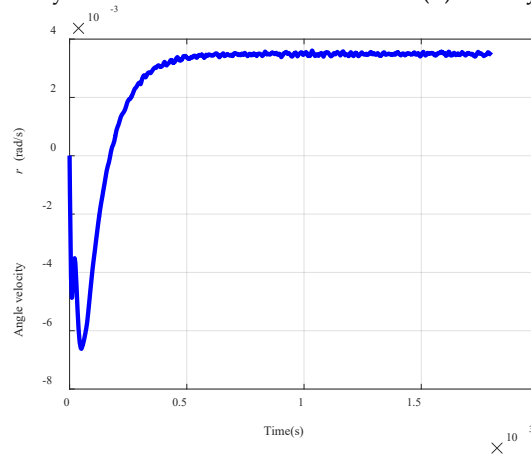
(c) Angle error.

**Figure 4.** Tracking errors in  $x$ ,  $y$ , and  $\psi$  of controlled AUSV: proposed method, blue solid line; desired trajectory, black dashed line.



(a) History of velocity in  $x$  axis.

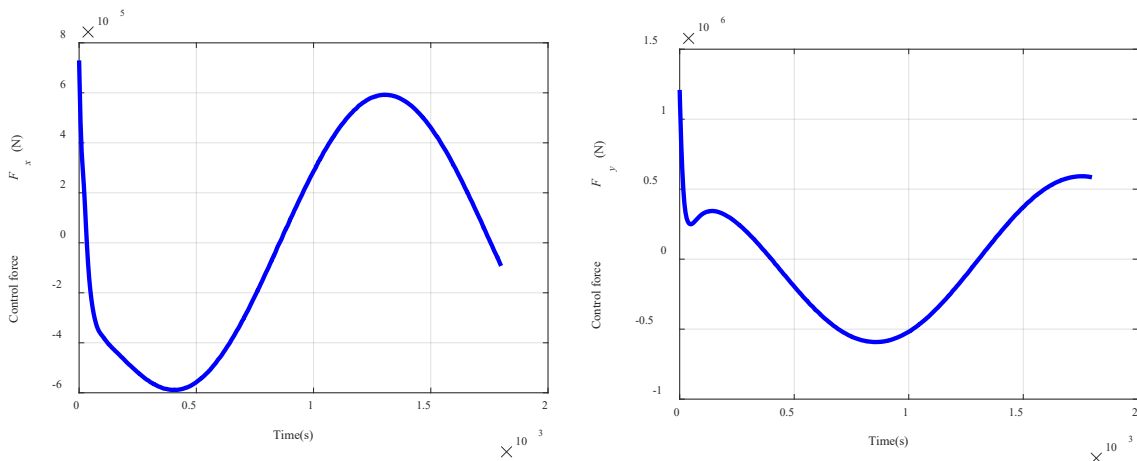
(b) History of velocity in  $y$  axis.



(c) History of rotation velocity in  $z$  axis.

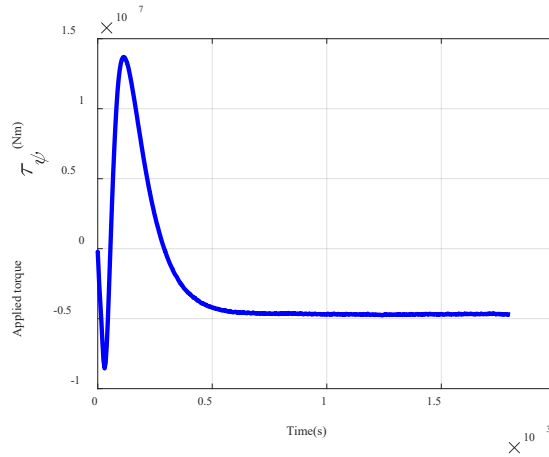
**Figure 5.** Histories of rotation velocities of controlled AUSV.

Applied control forces and torque are illustrated in Figure 6, which shows that control efforts  $F_x$  and  $F_y$ , and applied yaw torque  $\tau_\psi$  are bounded within  $\pm 0.8 \times 10^6$  N,  $\pm 1.3 \times 10^6$  N, and  $\pm 1.5 \times 10^7$  nm. These control commands are within a reasonable range in a marine environment.



(a) History of applied control force  $F_x$ .

(b) History of applied control force  $F_y$ .



(c) Applied yaw torque  $\tau_\psi$ .

Figure 6. Control commands of controlled AUSV.

**Scenario 2:** In this scenario, the desired path is generated with eight waypoints:  $WP_1$ : (0,200),  $WP_2$ : (300,500),  $WP_3$ : (700,500),  $WP_4$ : (1000,200),  $WP_5$ : (1000,-200),  $WP_6$ : (700,-500),  $WP_7$ : (300,-500),  $WP_8$ : (0,-200), and  $WP_9$ : (0,0).

Line-of-sight (LOS) angle between controlled AUSV and each waypoint can be calculated by using the following equation:

$$\psi_d = \tan^{-1} \left( \frac{y_d - y}{x_d - x} \right). \tag{32}$$

Figure 7 demonstrates the history of the waypoint-tracking result, indicating how the AUSV controlled via our proposed optimal method successfully tracks waypoint-generated trajectory, and how it turns automatically at each waypoint, i.e.,  $WP_i$  for  $i = 1, \dots, 9$ .

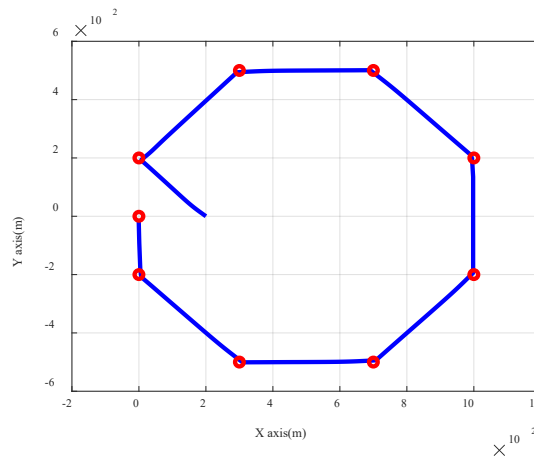
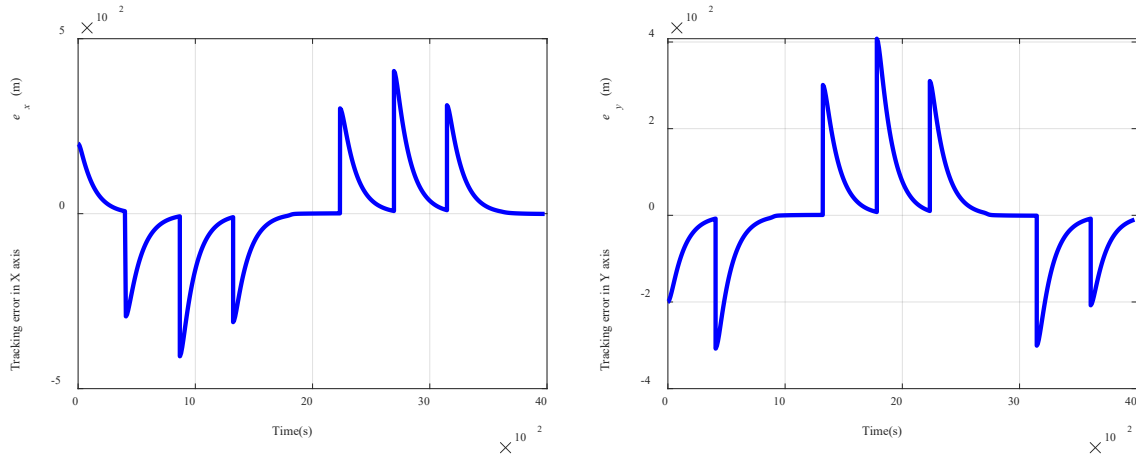


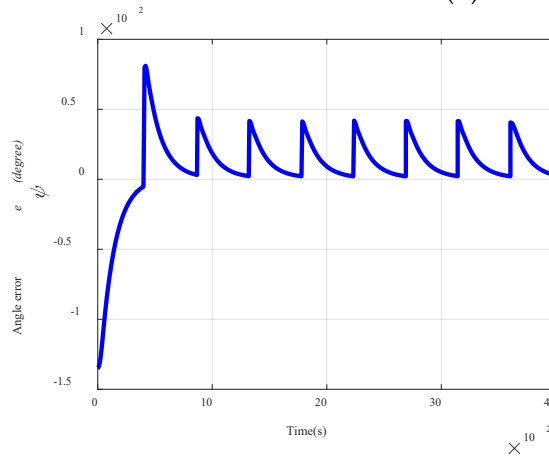
Figure 7. Waypoint-tracking result.

Histories of tracking errors in tracking each waypoint are illustrated in Figure 8, where the exponential convergent properties of tracking errors are revealed by applying this proposed optimal method.



(a) Tracking error in x axis.

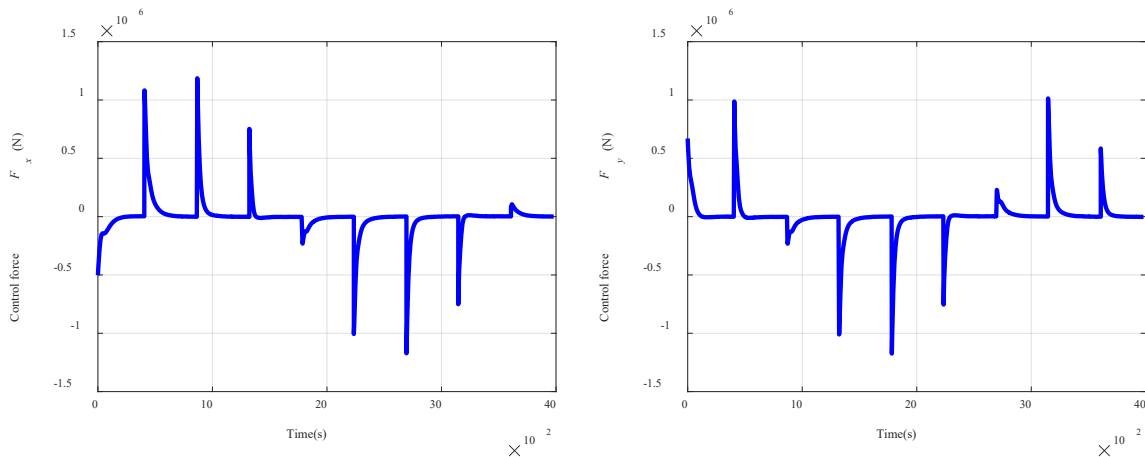
(b) Tracking error in y axis.



(c) Yaw angle tracking error.

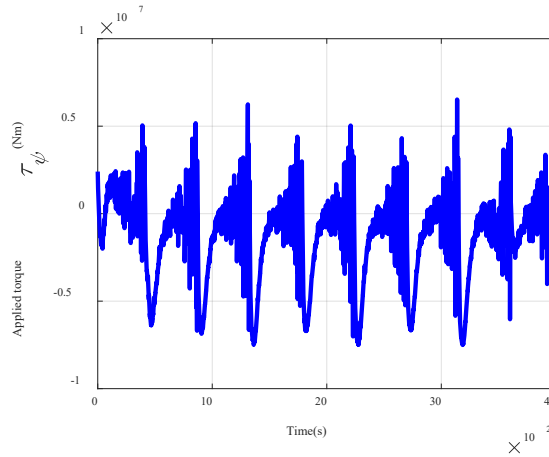
Figure 8. Tracking errors between controlled AUSV and waypoints.

Figure 9 shows how control efforts  $F_x$  and  $F_y$ , and applied yaw torque  $\tau_\psi$  were bounded within  $\pm 1.3 \times 10^6$  N,  $\pm 1.5 \times 10^6$  N, and  $\pm 7 \times 10^6$  nm. These control commands are within a reasonable range in a marine environment.



(a) History of control force  $F_x$ .

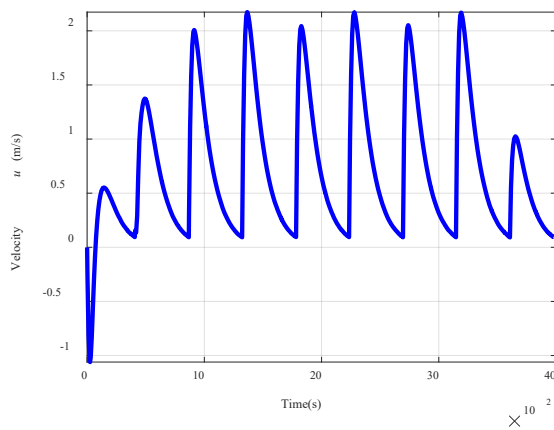
(b) History of control force  $F_y$ .



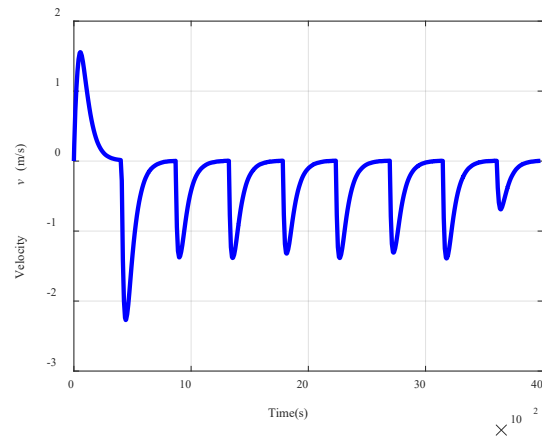
(c) Applied yaw torque  $\tau_\psi$ .

**Figure 9.** Control commands of controlled AUSV.

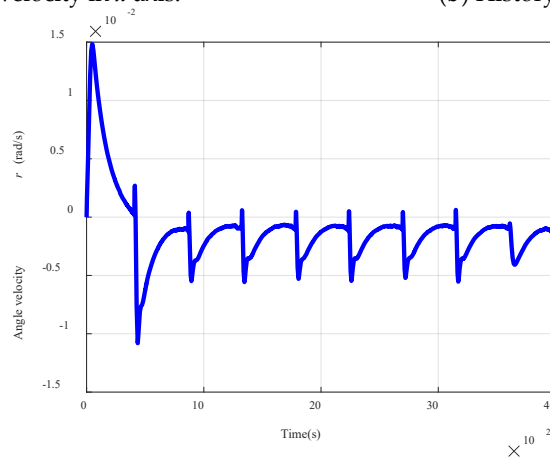
Histories of velocities of the controlled AUSV, including velocities ( $u$ ,  $v$ ) in axis  $x$  and  $y$  and rotation angle velocity  $r$  are shown in Figure 10.



(a) History of velocity in  $x$  axis.



(b) History of velocity in  $y$  axis.



(c) History of rotation-angle velocity in  $z$  axis.

**Figure 10.** Histories of velocities of controlled AUSV.

From the above analysis, simulation results of this proposed optimal control law revealed promising trajectory-tracking performance for the continuous trajectory and waypoints scenarios, even under the effects of time-varying ocean disturbances induced by wave, current, and wind, and random 5%–10% uncertain modelling uncertainties.

**5. Comparisons of Tracking Performance with Respect to Different Control gains:  $a_2$**

Optimal control gain  $a_2$  in Equation (29) is an adjustable parameter. Hence, in this section, trajectory- and waypoint-tracking performances with respect to different control gain  $a_2$  are analyzed. From the simulation result in Figure 11, tracking performance for the continuous circular trajectory is demonstrated. This scenario was successfully achieved for different control gains  $a_2$ . In the continuous case, tracking errors exponentially converged to zero. The observations of tracking errors and control commands, as shown in Figures 12, and 13 indicate that a small  $a_2$  resulted in quicker convergence rates in tracking the desired trajectory. Meanwhile, larger control commands could be found. In the discrete case, tracking performance for the discrete waypoints is demonstrated in Figure 14. This scenario was also successfully achieved for different control gains  $a_2$ . The tracking errors exponentially converged to zero as shown in Figure 15. In Figures 15 and 16, the tracking errors and control commands indicate that a small  $a_2$  resulted in quicker convergence rates in tracking the desired waypoints. Meanwhile, larger control commands could be found. These simulation results consisted of the inversely proportional property of the proposed nonlinear optimal control law, as seen in Equations (28) and (29), with respect to control gain  $a_2$ .

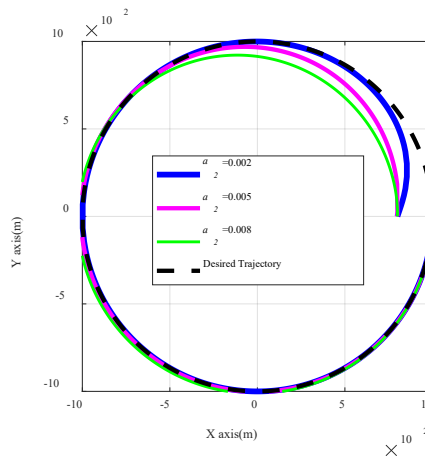
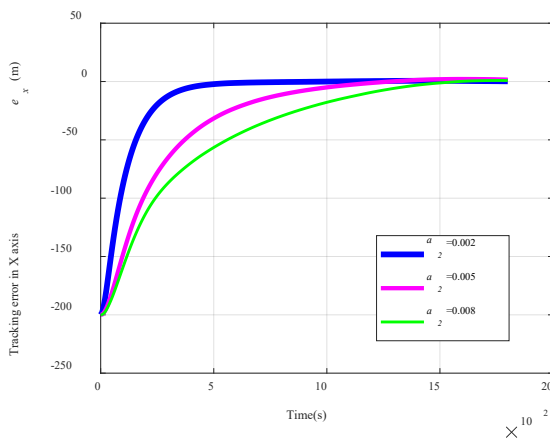
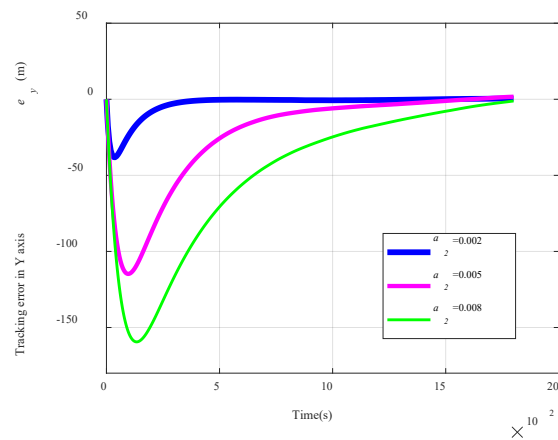


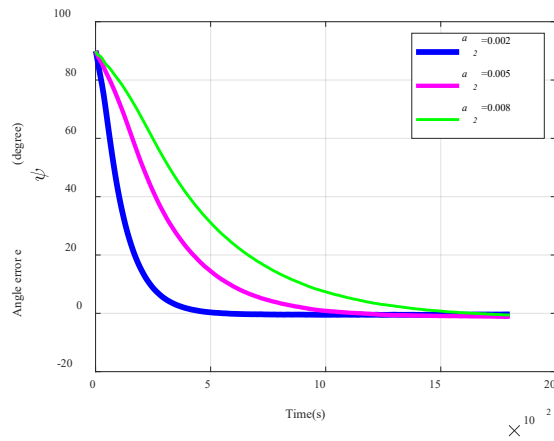
**Figure 11.** Tracking histories of controlled AUSV with respect to different control gains  $a_2$ .



**(a)** Tracking error in x axis.

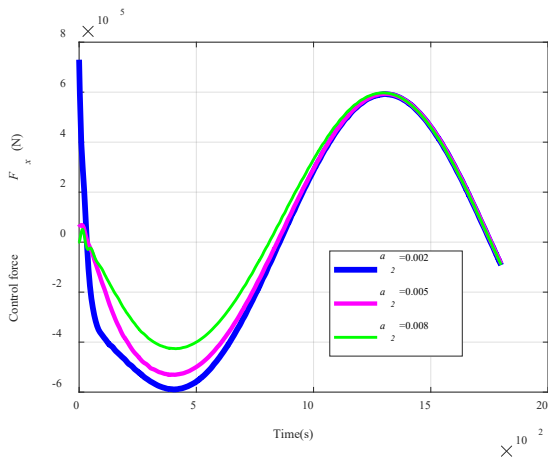


**(b)** Tracking error in y axis.

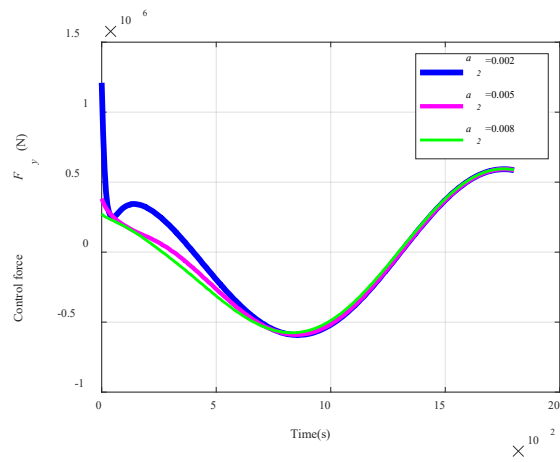


(c) Yaw angle error.

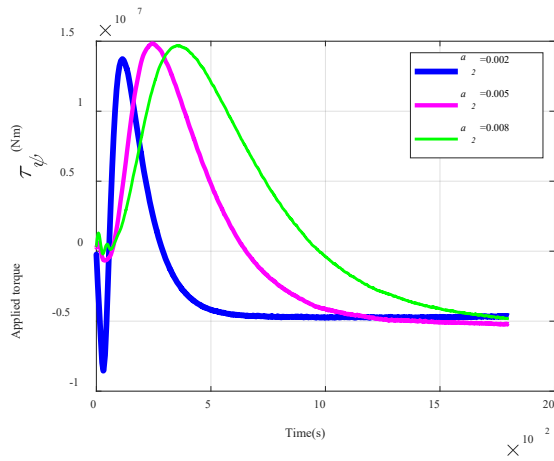
Figure 12. Tracking errors of controlled AUSV with respect to different control gains  $a_2$ .



(a) History of control force  $F_x$ .



(b) History of control force  $F_y$ .



(c) Applied torque  $\tau_\psi$

Figure 13. Control commands of controlled AUSV with respect to different control gains  $a_2$ .

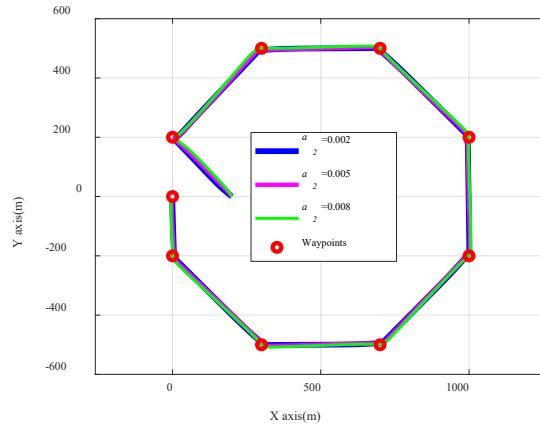
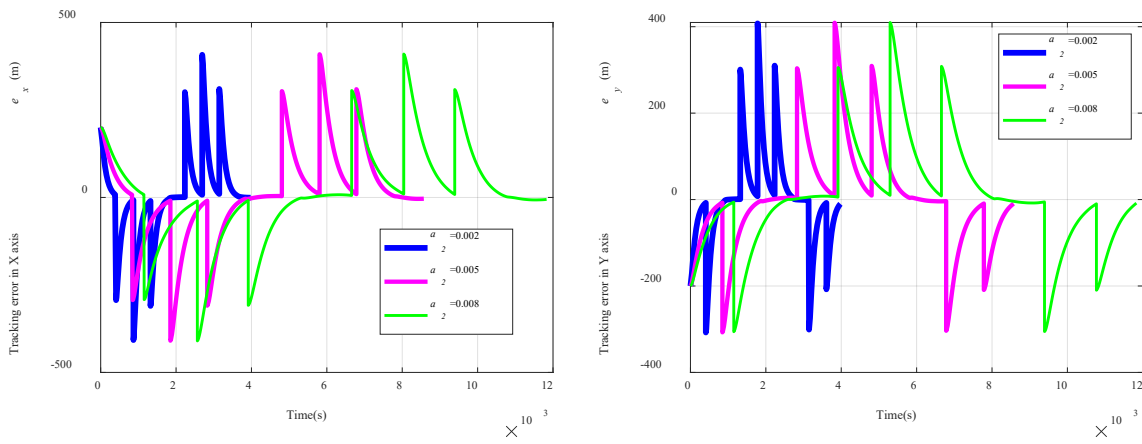
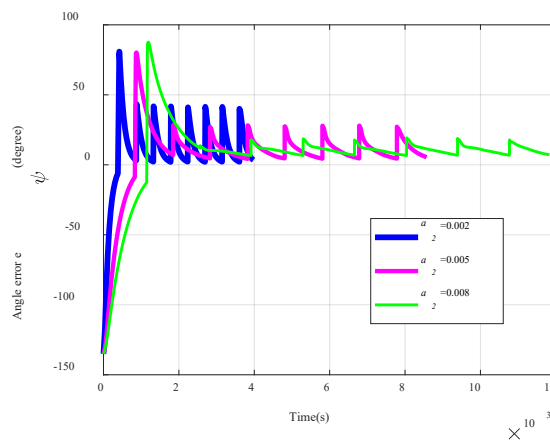


Figure 14. Tracking courses: waypoint-tracking scenario with respect to different control gains  $a_2$ .



(a) Tracking error in x axis.

(b) Tracking error in y axis.



(c) Yaw angle error.

Figure 15. Tracking errors of controlled AUSV with respect to different control gains  $a_2$ .

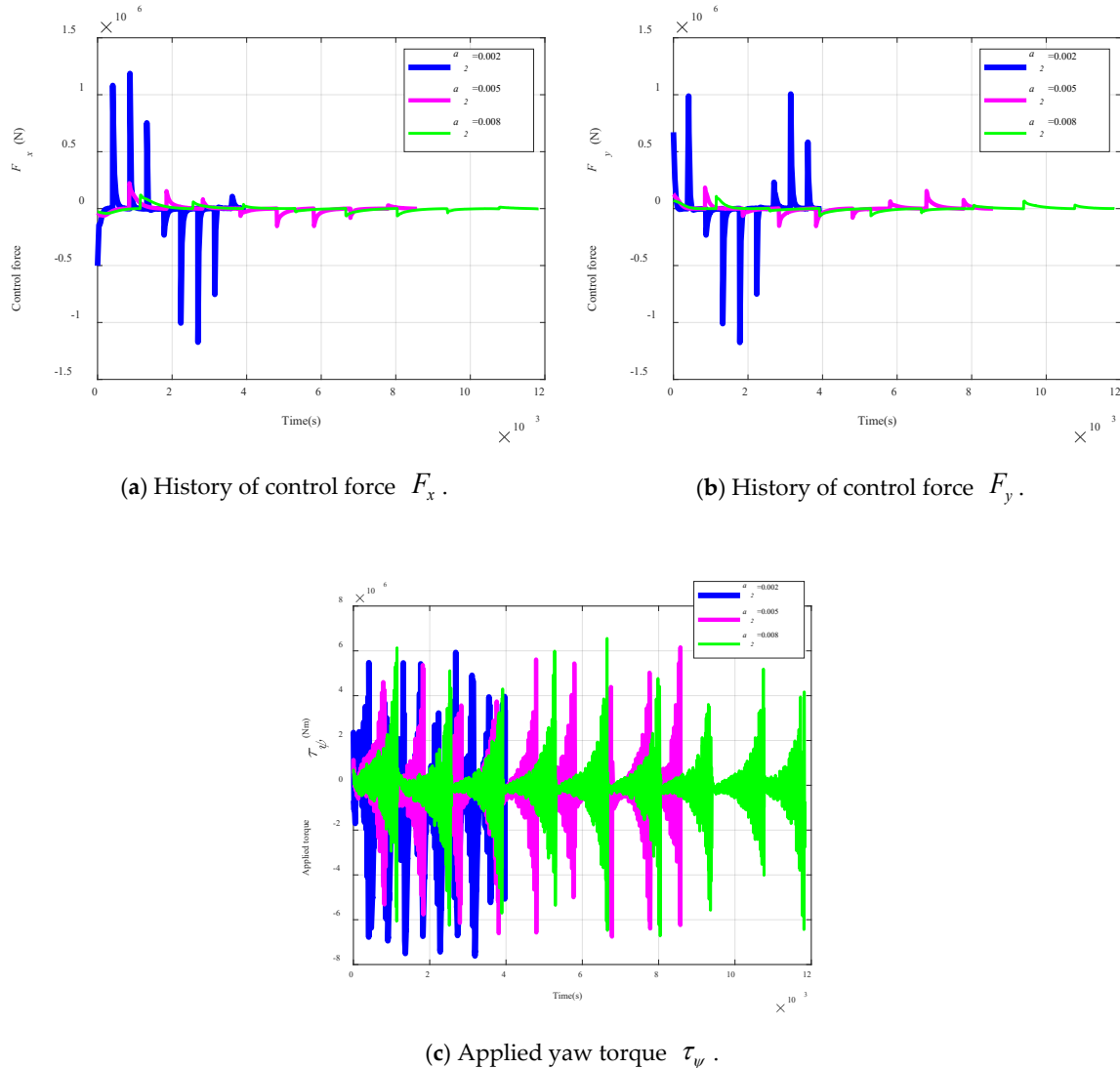


**Figure 16.** Control commands of controlled AUSV with respect to different control gains  $a_2$ .

The run time of the proposed control method with respect to the two testing scenarios is revealed in Table 7. In this study, the central processing unit (CPU) of the calculator used for calculating the proposed nonlinear optimal control law was Intel Core i7-8750H, 2.20 GHz. From Table 7, it is easy to find that the proposed nonlinear optimal control law can be executed in real time. This is because an average run time of 3 and 2 microseconds is spent for each single calculation of the proposed nonlinear optimal control law with respect to the trajectory and waypoint scenarios, respectively.

**Table 7.** Run time of proposed control method with respect to two testing scenarios.

Scenario 1: circular trajectory	Average run time: $2.6547 \times 10^{-6}$ s.
Scenario 2: waypoints	Average run time: $2.0099 \times 10^{-6}$ s.

## 6. Conclusions

A nonlinear optimal control law for the trajectory- and waypoint-tracking problem of AUSVs was presented in this investigation. One of the main contributions of this investigation was analytically solving the closed-form solution for the nonlinear optimal trajectory-tracking problem of AUSVs. In general, it is difficult to find the closed-form solution for this problem due to the high dimension and complexity of the controlled AUSV. The concise form of the derived closed-form

solution is easy to implement and a low computational burden for the proposed nonlinear optimal control law. From the simulation results of the two scenarios, promising trajectory- and waypoint-tracking abilities were revealed by this proposed nonlinear optimal control law, even under marine-environment disturbances and modelling uncertainties.

**Author Contributions:** Yung Yue Chen proposed the main idea and wrote the paper. Chun-Yen Lee, and Shao-Han Tseng designed and performed the experiments together. Yung Yue Chen and Wei-Min Hu analyzed the results. All authors have read and agreed to the published version of the manuscript.

**Funding:** This work was financially supported by National Science Council, Taiwan, R.O.C. (Grant No. NSC101-2221-E-006-45-MY3).

**Conflicts of Interest:** The author(s) declared no potential conflicts of interest with respect to the research, authorship, and/or publication of this article.

## Appendix A

Consider cost function  $J_2(\mathbf{u}_2)$ , and it is obvious that Equation (11) can be rewritten as:

$$J_2(\mathbf{u}_2) = \mathbf{e}^T(0)\mathbf{P}_2(\mathbf{e}(0), 0)\mathbf{e}(0) + \int_0^{t_f} [\mathbf{e}^T(t)(\dot{\mathbf{P}}_2(\mathbf{e}, t) + \mathbf{P}_2(\mathbf{e}, t)\mathbf{R}_{2V}(\mathbf{e}, t) + \mathbf{R}_{2V}^T(\mathbf{e}, t)\mathbf{P}_2(\mathbf{e}, t) + \mathbf{Q}_2)\mathbf{e}(t) + \mathbf{u}_2^T(t)\mathbf{W}_2\mathbf{u}_2(t) + \mathbf{u}_2^T(t)\mathbf{S}_{2V}(\mathbf{e}, t)\mathbf{P}_2(\mathbf{e}, t)\mathbf{e}(t) + \mathbf{e}^T(t)\mathbf{P}_2(\mathbf{e}, t)\mathbf{S}_{2V}(\mathbf{e}, t)\mathbf{u}_2(t)] dt \quad (\text{A1})$$

Using the nonlinear differential equation in Equation (13), it yields

$$J_2(\mathbf{u}_2, 0) = \mathbf{e}^T(0)\mathbf{P}_2(\mathbf{e}(0), 0)\mathbf{e}(0) + \int_0^{t_f} \left[ (\mathbf{u}_2(t) + \mathbf{W}_2^{-1}\mathbf{S}_{2V}^T(\mathbf{e}, t)\mathbf{P}_2(\mathbf{e}, t)\mathbf{e}(t))^T \mathbf{W}_2 (\mathbf{u}_2(t) + \mathbf{W}_2^{-1}\mathbf{S}_{2V}^T(\mathbf{e}, t)\mathbf{P}_2(\mathbf{e}, t)\mathbf{e}(t)) \right] dt \quad (\text{A2})$$

Choosing  $\mathbf{u}_2$  as that in Equation (12), the following result can be obtained:

$$J_2(\mathbf{u}_2^*(\mathbf{e}, t)) = \min_{\mathbf{u}_2(t) \in L_2[0, t_f]} J(\mathbf{u}_2) = \mathbf{e}^T(0)\mathbf{P}_2(\mathbf{e}(0), 0)\mathbf{e}(0) \quad (\text{A3})$$

This is the optimal control performance in Equation (11).

## References

- Papoulias, F.A. Cross track error and proportional turning rate guidance of marine vehicles. *J. Ship Res.* **1994**, *38*, 123–132.
- Vukic, Z.; Ozbolt, H.; Pavlekovic, D. Improving fault handling in marine vehicle course-keeping systems. *IEEE Proc. Robot. Autom. Mag.* **1999**, *6*, 39–52.
- Temel, T.; Ashrafiuon, H. Sliding-mode speed controller for tracking of underactuated surface vessels with extended Kalman filter. *Electron. Lett.* **2015**, *51*, 467–469.
- Valenciaga, F. A second order sliding mode path following control for autonomous surface vessels. *Asian J. Control* **2014**, *16*, 1515–1521.
- Kahveci, N.E.; Ioannou, P.A. Adaptive steering control for uncertain ship dynamics and stability analysis. *Automatica* **2013**, *49*, 685–697.
- Qiaomei, S.; Guang, R. An online adaptive logic-oriented neural approach for tracking control. *Ocean Eng.* **2013**, *58*, 106–114.
- Ghommam, J.; Mnif, F.; Derbel, N. Global stabilisation and tracking control of underactuated surface vessels, *IEEE Control Theory Appl.* **2010**, *4*, 71–88.
- Chen, X.; Tan, W.W. Tracking control of surface vessels via fault-tolerant adaptive back stepping interval type-2 fuzzy control. *Ocean Eng.* **2013**, *70*, 97–109.
- Serrano, M. E.; Godoy Bordes, S.A.; Gandolfo, D.; Mut, V.A.; Scaglia, G.J.E. Nonlinear Trajectory Tracking Control for Marine Vessels with Additive Uncertainties. *Inf. Technol. Control* **2018**, *47*, 118–130.
- Paliotta, C.; Lefeber, E.; Pettersen, K.Y.; Pinto, J.; Costa, M. Trajectory tracking and path following for underactuated marine vehicles. *IEEE Trans. Control Syst. Technol.* **2019**, *27*, 1423–1437.
- Serrano, M.E.; Scaglia, G.; Godoy, S.A.; Mut, V.; Ortiz, O.A. Trajectory tracking of underactuated surface,

- vessels: A linear algebra approach. *IEEE Trans. Control Syst. Technol.* **2014**, *22*, 1103–1111.
12. Bertaska, I.R.; Shah, B.; von Ellenrieder, K.; Švec, P.; Klinger, W.; Sinisterra, A.J.; Dhanak, M.; Gupta, S.K. Experimental evaluation of automatically-generated behaviors for USV operations. *Ocean Eng.* **2015**, *106*, 496–514.
  13. Fossen, T.I.; Sagatun, S.I.; Sorensen, A.J. Identification of dynamically positioned ships. *Control Eng. Pract.* **1996**, *4*, 369–376.



© 2020 by the authors. Licensee MDPI, Basel, Switzerland. This article is an open access article distributed under the terms and conditions of the Creative Commons Attribution (CC BY) license (<http://creativecommons.org/licenses/by/4.0/>).